Journal of Microscopy, Vol. 210, Pt 3 June 2003, pp. 234–240
Received 10 August 2002; accepted 25 October 2002

Near-field Raman spectroscopy using a sharp metal tip

A. HARTSCHUH, N. ANDERSON & L. NOVOTNY
The Institute of Optics, University of Rochester, Wilmot Building, Rochester, NY 14627, U.S.A.

Key words. Carbon nanotubes, near-field microscopy, surface-enhanced Raman scattering.

Summary

Near-field Raman spectroscopy with a spatial resolution of 20 nm is demonstrated by raster scanning a sharp metal tip over the sample surface. The method is used to image vibrational modes of single-walled carbon nanotubes. By combining optical and topographical signals rendered by the single-walled carbon nanotubes, we can separate near-field and far-field contributions and quantify the observed Raman enhancement factors.

Introduction

Combined with near-field techniques, Raman spectroscopy is a promising tool for identifying and analysing the molecular composition of complex materials, providing spatially resolved chemical maps with nanoscale resolution. A basic drawback of Raman methods is the comparatively low scattering cross-section precluding the detection of single scatterers. However, this drawback can be overcome using surface-enhanced Raman scattering (SERS) induced by nanometre-sized metal structures. SERS has been shown to provide enormous enhancement factors of up to 10^{15} allowing for Raman spectroscopy at even the single molecule level (Kneipp *et al.*, 1997; Nie & Emory, 1997).

SERS has been known for more than 20 years, however, the contributing mechanisms are still not fully understood. The strongest contribution is of electromagnetic origin, caused by the enhancement of the local field E_{local} with respect to the incident field E_0. The electromagnetic enhancement factor M, defined as the ratio between measured Raman cross-section in the presence and the absence of the metal surface, scales approximately with the fourth power of the ratio of these fields $[M \approx (E_{local}/E_0)^4]$ and is reported to reach up to 12 orders of magnitude for particular multiple particle configurations involving interstitial sites between particles or outside sharp surface protrusions (Xu *et al.,* 2000). For a single spherical particle M is supposed to be much lower, in the range 100–1000.

Correspondence to: A. Hartschuh. Fax: +1 585 244 4936; e-mail: hartschu@optics.rochester.edu

By placing a laser illuminated ultra-sharp metal tip on top of the sample surface, we intend to limit SERS to the volume close to the very end of the tip. Raster scanning the sample should then allow for Raman imaging with nanometre resolution (Wessel, 1985). Raman enhancement using metal tips has been shown previously (Stöckle *et al.*, 2000; Hayazawa *et al.*, 2001, 2002; Nieman *et al.*, 2001). Here, we demonstrate its unique high-resolution imaging capability.

Single-walled carbon nanotubes (SWNTs) are promising new materials with a wide range of potential applications. The unique properties of SWNTs arise from their particular one-dimensional structure which is directly linked to characteristic Raman bands. Structural properties, such as chirality or local defects, affect both the Raman signal and desired features (e.g. electric conductivity; Rao *et al.*, 1997). Raman signals of SWNTs have been studied intensively in the literature (see e.g. Duesberg *et al.*, 2000; Jorio *et al.*, 2001; Yu & Brus, 2001; Maultzsch *et al.*, 2002) and signal enhancements of up to 10^{12} have been reported for tubes in contact with fractal silver colloidal clusters (Kneipp *et al.*, 2000).

The size of SWNTs offers the possibility to localize scatterers topographically and to detect the corresponding Raman signal simultaneously. With this information we can separate near-field and far-field contributions and quantify the observed enhancement factors.

Materials and methods

Our experimental set-up is shown schematically in Fig. 1. The output of a HeNe laser at 633 nm (P = 15 mW, TEM_{00}) was expanded, attenuated to 30–100 μW and sent into the microscope. The beam passed a laser line filter, was reflected by a dichroic beamsplitter and focused by a high numerical aperture objective (1.4 NA) onto the sample surface. The Raman-scattered light was collected with the same objective, transmitted by the beamsplitter and filtered by a longpass filter. The signal was detected either by a combination of a spectrograph and an intensified charge coupled device, or by a photon-counting avalanche photodiode after spectral filtering using a narrow bandpass filter [full width at half maximum (FWHM) = 10 nm] centred at 760 or 700 nm, respectively.

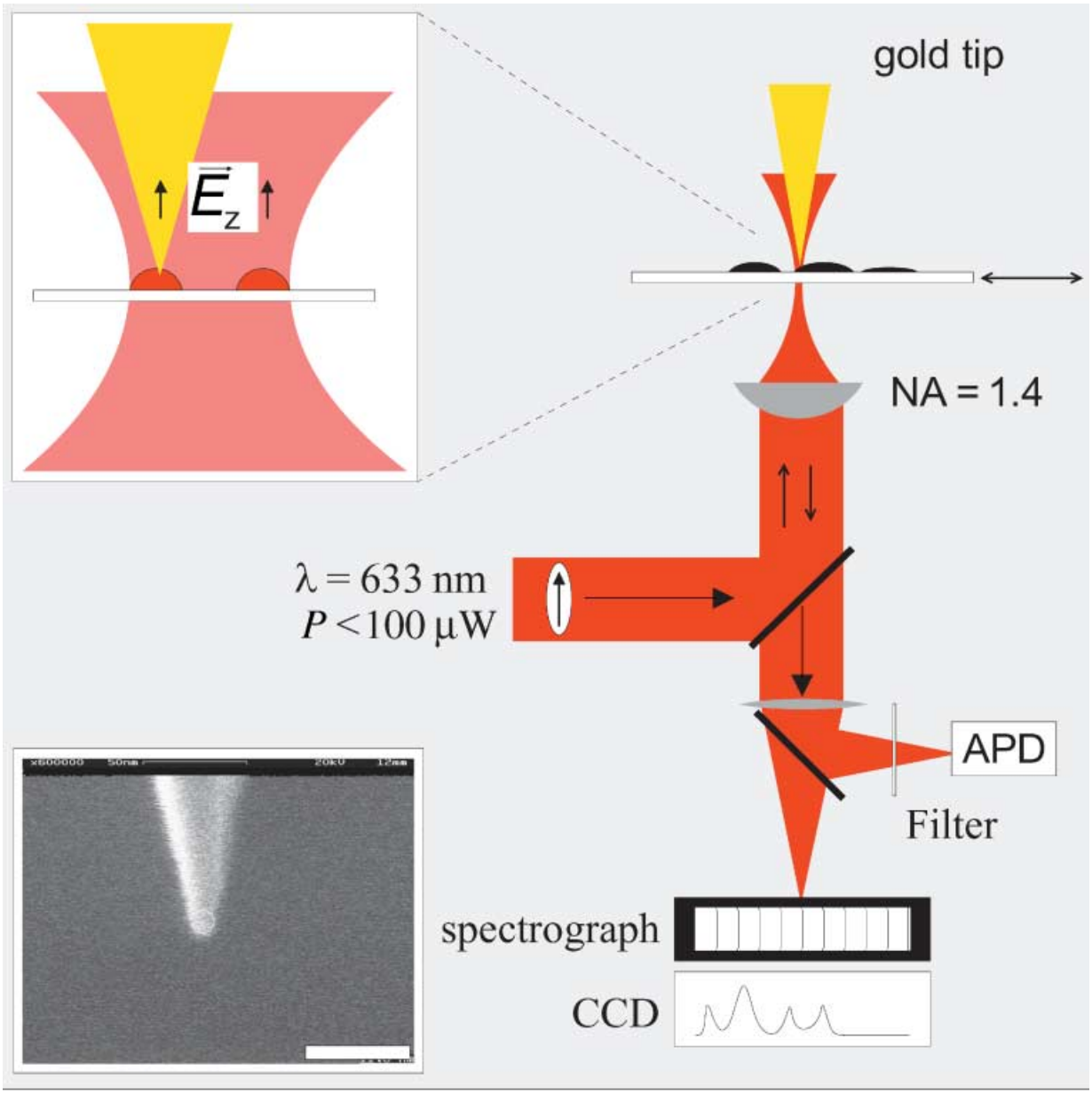

Fig. 1. Experimental set-up. (Inset upper left) Distribution of the longitudinal electric field $\vec{E}_z$ within a tightly focused laser beam (schematic) (Sick *et al.*, 2000). (Inset lower left) Scanning electron micrograph of an ultra-sharp gold tip produced by electrochemical etching. Scale bar, 50 nm.

The metal tip is held within 1 nm of the sample surface by using a tuning-fork feedback mechanism (Karrai & Grober, 1995). Typical interaction forces between tip and sample are in the range 10–50 pN, small enough not to affect the tip shape. This soft interaction is achieved by using a tuning fork with high quality factor for oscillation and by keeping the frequency detuning constant with a digital phase-locked loop.

The metal tip is placed in the centre of one of the lobes with longitudinal field components produced by a tightly focused Gaussian beam (Sick *et al.*, 2000) (see inset upper left in Fig. 1) and needed for the generation of the field enhancement (Novotny *et al.*, 1998; Sánchez *et al.*, 1999). Sharp gold tips with a radius of curvature around 15 nm are produced by electrochemical etching with HCl (see inset lower left in Fig. 1).

Purified SWNTs with a diameter distribution of 1.0–1.5 nm, produced by arc-discharge using nickel/yttrium catalyst particles, were used as purchased from Bucky USA. The material was dispersed in dichlorethane, sonicated for 1 h and spin-cast on a microscope cover glass. The sample was mounted on a 40 × 40 μm closed-loop scan bed.

Results and discussion

Coverage of our SWNT samples was first determined by

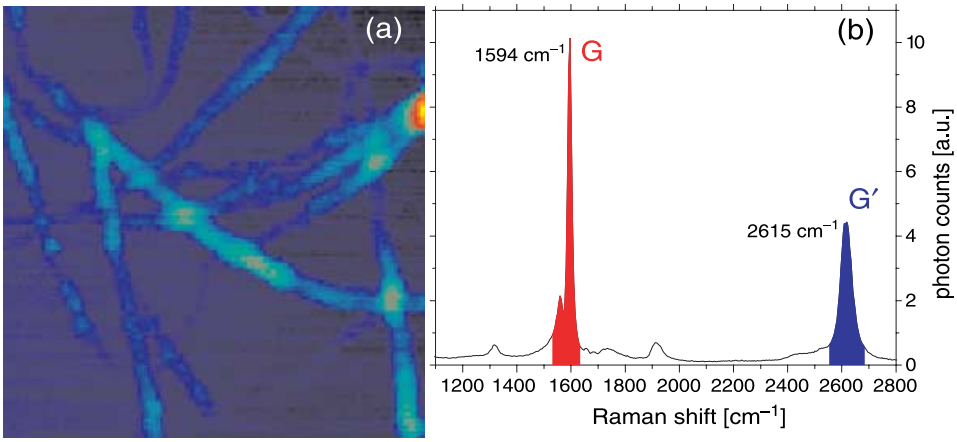

Fig. 2. (a) Topographic image of SWNT bundles on glass. Scan area 1 × 1 μm. Maximum height of the bundles is 30 nm. (b) Typical far-field Raman spectrum detected for bundles of SWNTs upon laser excitation at 633 nm. The characteristic Raman bands G (at 1596 cm^{-1}) and G′ (at 2615 cm^{-1}) are marked to indicate the range used for spectral integration in Figs 4, 5, 6 and 7.

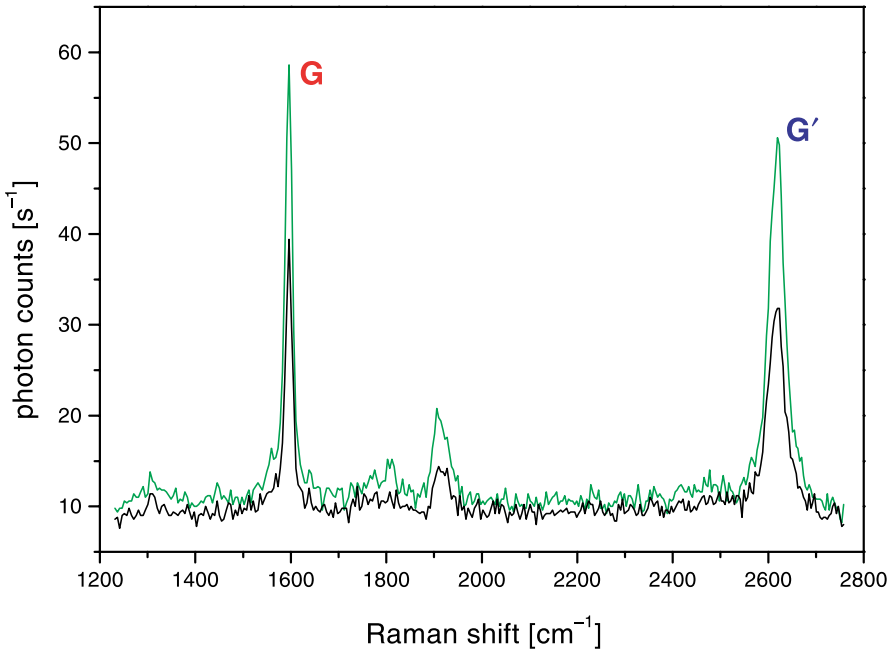

Fig. 3. Raman spectra detected with a sharp metal tip (green line) on top of the sample (distance ≈ 1 nm) and with the tip retracted by 2 μm (black line). Note, the intensities of all Raman bands are increased with the tip close to the SWNTs.

atomic force microscopy and confocal far-field measurements. Figure 2(a) shows a typical topographic image revealing the characteristic one-dimensional features of SWNTs.

The non-uniform height and width of these features indicate that the tubes form over-lapping bundles that consist of varying numbers of single tubes. Far-field Raman spectra detected for these bundles (Fig. 2b) exhibit the characteristic bands of SWNTs: the sharp G band at 1596 cm^{-1}, caused by the tangential stretching mode, and the broader G′ band at 2615 cm^{-1}, which originates from a double resonance Raman scattering process (Souza Filho *et al.*, 2002).

In Fig. 3 the spectra of a different sample area in the presence of a sharp metal tip (green line) and with the tip retracted by 2 μm (black line) are presented. All Raman bands appear stronger with the tip close to the SWNTs (distance ≈ 1 nm). Importantly, the positions and relative intensities of the different Raman bands remain unchanged and no additional bands are observed. Hence, we have no indication for an electric field gradient effect discussed in Ayars *et al.* (2000).

In the following, Raman images are established by raster scanning the sample and simultaneous detection of the intensities within the spectral ranges of the two bands indicated in Fig. 2(b). Figure 4(a) presents a Raman image acquired while raster scanning a sharp metal tip on top of the surface. The optical signal was detected by the APD combined with a narrow bandpass filter allowing for a short integration time of 5 ms per pixel. The bandpass filter was centred at 760 nm (FWHM = 10 nm) transmitting only light within the spectral

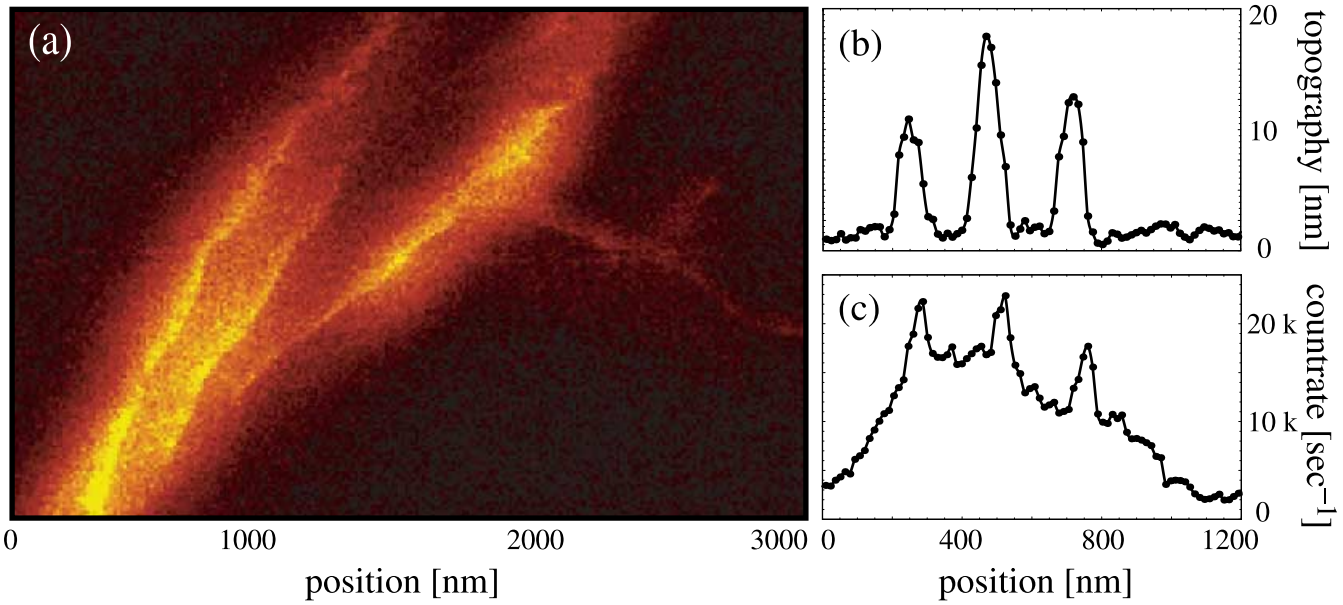

Fig. 4. (a) Raman image of SWNT bundles acquired by raster scanning a sharp metal tip and detecting the intensity of the G′ band (scan area 3×1 μm, integration time 5 ms per pixel). (b and c): Cross-sections taken along the white dotted line in (a) for topography (b) and Raman signal (c).

range of the G′ band (see Fig. 2b). Similar images were observed by detecting the intensity of the G band using a bandpass filter at 700 nm.

The Raman image in Fig. 4(a) shows three bright stripes leading from the lower left towards the upper right of the image. In Fig. 4(b,c) cross-sections of the optical and the corresponding topographical image taken along the dotted white line in (Fig. 4a) are presented. The topography scan exhibits three separated bundles of SWNTs with a height between 10 and 15 nm. The position of theses bundles coincides with the sharp peaks in the Raman signal shown in (c) and (a) which occur only in the presence of the tip. The width of these peaks is around 30 nm – far below the diffraction limit for the detected wavelength of 760 nm. Hence, we observe near-field signals from SWNTs enhanced by the metal tip. The sharp near-field contributions in Fig. 4(a and c) sit on top of broad contributions which do not depend on the tip position and are caused by the far-field.

Images established by measuring complete spectra at every pixel and numerical integration of the signals in the spectral range of the G and G′ bands are shown in Fig. 5(c–f) together with the corresponding topographic images in Fig. 5(a and b). All Raman images (c–f) exhibit long, but sharp, features which correspond to the topographic signatures of the SWNT bundles present in (a) and (b). Hence, these features are caused by the Raman signals of SWNTs. The widths of the optical features are in the range 20–100 nm, far below the diffraction limit for the observed wavelength.

In order to verify the near-field origin of the image contrast, we studied the dependence of the signal enhancement on the tip–sample distance. In Fig. 6 the signal intensity of the G′ band is plotted from 1 to 200 nm. For separations larger than 30 nm the observed signal remains virtually unchanged resulting purely from far-field components. However, for smaller distances, a steep increase in the signal occurs indicating a distance-dependent near-field contribution.

For an evaluation of the actual enhancement factors (ratio between Raman signal with and without tip), the exact number and position of the contributing Raman scatterers has to be known. In the case of dye molecules, this can not usually be determined (Stöckle *et al.*, 2000; Hayazawa *et al.*, 2001, 2002). Furthermore, far-field and near-field contributions have to be separated, which is not possible for dense samples with overlapping far-field contributions as in Fig. 4(c).

Figure 7 shows a line scan of a different sample area containing only one isolated bundle. Topography scans of the surrounding area (1×1 μm) made sure no further tubes contribute to the far-field signal. The optical signal in Fig. 7 exhibits two different contributions: the sharp near-field peak centred at 330 nm and the much broader peak caused by the far-field. The total signal can be described by a sum of two Gaussian curves (red line in Fig. 7) representing the near-field (FWHM = 26 nm) and far-field (FWHM = 330 nm) contribution, respectively.

In the case of Fig. 7, the signal with the near-field contribution caused by the tip is only a factor of 2.3 higher than without the tip. However, for an evaluation of the enhancement factor, the different volumes which are probed by near-field and far-field components must be taken into account. Based on the topographical information this volume can be estimated. The topography scan in Fig. 7 (inset) shows the height of the bundle to be $h \approx 10$ nm. The observed width of 35 nm

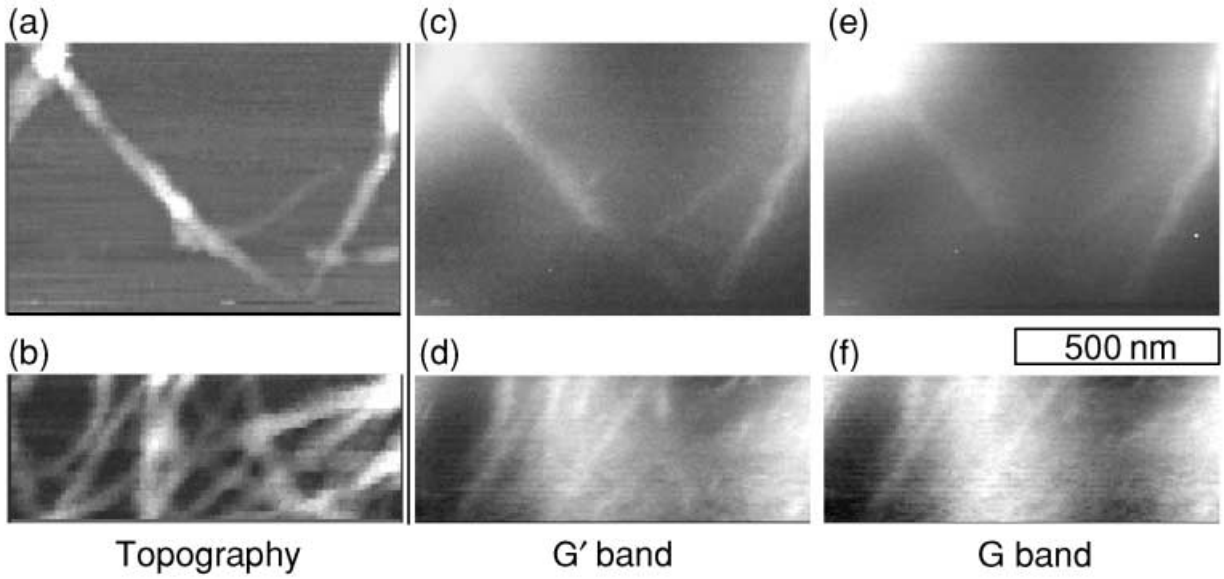

Fig. 5. (a and b) Topographic images of SWNT bundles (max. height 20 nm). (c–f) Raman images of the same area acquired by detecting the intensities of the Raman bands G′ and G (cf. Fig. 2b). 50 ms integration time per pixel. All images have a width of 1 μm.

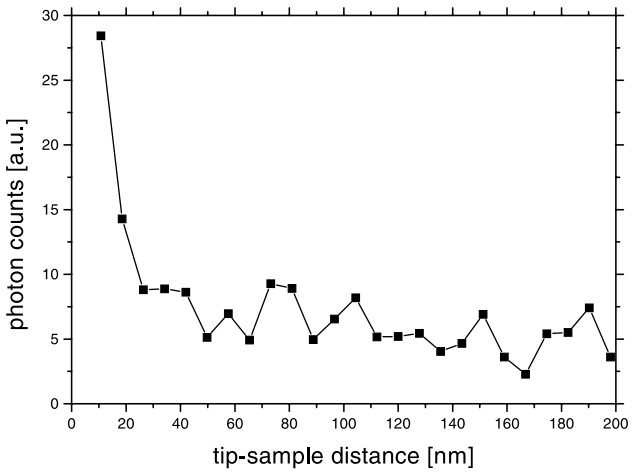

Fig. 6. Intensity of the Raman band G′ of SWNTs as a function of the tip–sample distance. The steep increase for separations smaller than 20 nm indicates tip-enhanced Raman scattering in the near-field.

will be affected by the finite size of the probing metal tip. A reasonable estimate for the actual width of the bundle would be lower, around $w = 20$ nm. The length of the bundle is larger than the width of the focus ($f = 330$ nm) resulting in a probed volume of $\approx h \times w \times f = 10\ \text{nm} \times 20\ \text{nm} \times 330\ \text{nm} = 66\,000\ \text{nm}^3$. In the case of the near-field, a much smaller volume is probed. Using the width of the observed near-field peak of 26 nm results in $10\ \text{nm} \times 20\ \text{nm} \times 26\ \text{nm} = 5200\ \text{nm}^3$. Normalizing the observed signal contributions in Fig. 7 of 200 and 160 for the near-field and far-field with the ratio of the detected volumes yields an enhancement factor of $M = 16$. For two reasons, this value represents only a lower limit. The estimate for the volume being probed in the near-field assumes a uniform enhancement for the complete thickness of the bundle ($h = 10$ nm). However, the distance dependence presented in Fig. 6 clearly shows a steep increase within the range of a few nanometres. The actual enhancement will originate mainly from the uppermost tubes reducing the probed volume by at least a factor of 2.

Furthermore, the field enhancement mechanism at the tip requires electric field components parallel to the tip axis (Novotny *et al.*, 1998; Sánchez *et al.*, 1999). However, for the on-axis illumination scheme and the Gaussian (0,0) mode used in our studies, only ≈ 10–20% of the total intensity is contained in either of the lobes with *z*-components (see Materials and methods). Hence, the field enhancement is caused by only 10–20% of the total field, whereas the remaining intensity causes the far-field. More favourable would be the application of higher order laser modes such as the Hermite–Gaussian (1,0) or the radially polarized Laguerre–Gaussian mode (Novotny *et al.*, 1998).

Taking these factors into account the actual enhancement factor is estimated to be around 200. While this factor is more than 10 orders of magnitude lower than the highest SERS values reported in literature, it is in the range expected for a single spherical gold particle with a radius of 10 nm and a sample-particle distance between 0.5 and 2.75 nm at $\lambda = 633$ nm (Xu *et al.*, 2000).

For our studies, we do not expect significant contributions from chemical effects based on charge-transfer processes between scatterer and metal or overlapping electron wavefunctions due to the large tip–sample separation of 1 nm.

Even though all metal tips were fabricated using the same procedure and appeared equally sharp in scanning electron

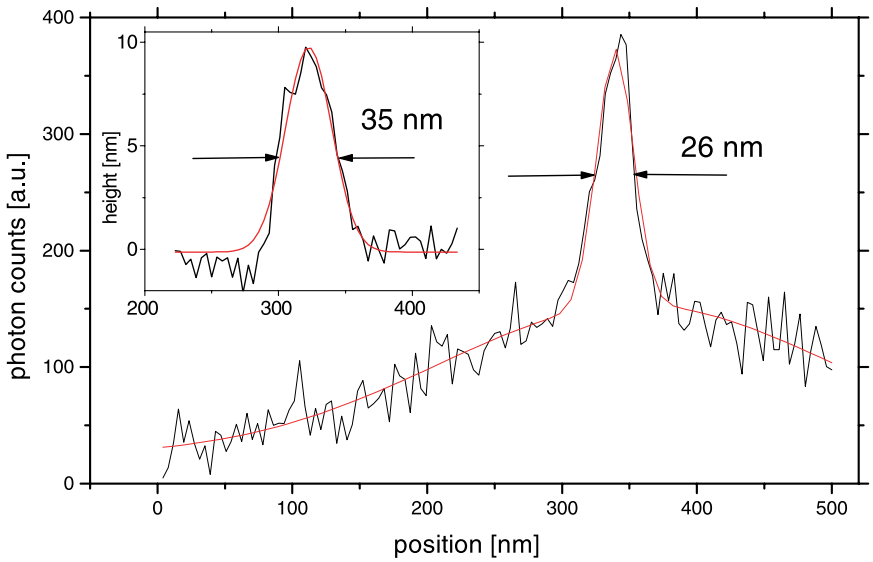

Fig. 7. Optical line scan of an isolated SWNT bundle integrating the intensity of the Raman band G′. The sharp near-field peak at ≈ 330 nm appears on top of a broad far-field contribution. (Red line) Fit curve consisting of two Gaussian peaks representing the near-field (FWHM = 26 nm) and far-field (FWHM = 330 nm) contribution. (Inset) Topography scan of the SWNT bundle indicating a height of ≈ 10 nm.

microscopy images, the observed enhancement factors varied from tip to tip. In fact, only 20–30% of the tips we studied produced an appreciable enhancement. The reason for this behaviour is the subject of ongoing studies.

Most importantly, the image contrast produced by the comparatively low enhancement factors we observed, already allows for a clear separation of nanometre-sized features as can be seen from Figs 4 and 5. From the images we acquired we can estimate the lower limit for detection of the tip-induced enhancement to be around 50.

Conclusion

Here, we have demonstrated vibrational imaging of SWNT bundles with 20 nm resolution by raster scanning a sharp metal tip over the sample surface. The size and characteristic structure of SWNTs offered the possibility to simultaneously localize scatterers topographically and to detect the corresponding enhanced Raman signals. By combining both sets of data, we were able to separate near-field and far-field contributions and to quantify the observed enhancement. Although the enhancement factors determined in our studies are much lower than the giant factors reported for particular surface structures and multiple particle configurations, they are in good agreement with theoretical predictions for single spherical particles.

Acknowledgements

The authors wish to thank M. Beversluis and A. Bouhelier for stimulating discussions and T. Krauss, J. Haremza and E. J. Sánchez for support in sample preparation. This work was funded by the National Science Foundation NSF through Grant BES-0086368.

References

Ayars, E.J., Hallen, H.D. & Jahncke, C.L. (2000) Electric field gradient effects in Raman spectroscopy. *Phys. Rev. Lett.* **85**, 4180–4183.

Duesberg, G.S., *et al.* (2000) Polarized Raman spectroscopy on isolated single-wall carbon nanotubes. *Phys. Rev. Lett.* **85**, 5436–5439.

Hayazawa, N., *et al.* (2001) Near-field Raman scattering enhanced by a metallized tip. *Chem. Phys. Lett.* **335**, 369–374.

Hayazawa, N., *et al.* (2002) Near-field Raman imaging of organic molecules by an apertureless metallic probe scanning optical microscope. *J. Chem. Phys.* **117**, 1296–1301.

Jorio, A., *et al.* (2001) Structural (n,m) determination of isolated single-wall carbon nanotubes by resonant Raman scattering. *Phys. Rev. Lett.* **86**, 1118–1121.

Karrai, K. & Grober, R.D. (1995) Piezoelectric tip–sample distance control for near field optical microscopes. *Appl. Phys. Lett.* **66**, 1842–1844.

Kneipp, K., *et al.* (1997) Single molecule detection using surface-enhanced Raman scattering (SERS). *Phys. Rev. Lett.* **78**, 1667–1670.

Kneipp, K., *et al.* (2000) Surface-enhanced and normal Stokes and anti-Stokes Raman spectroscopy of single-walled carbon nanotubes. *Phys. Rev. Lett.* **84**, 3470–3473.

Maultzsch, J., Reich, S. & Thomsen, C. (2002) Raman scattering in carbon nanotubes revisited. *Phys. Rev. B*, **65**, 233402–233406.

Nie, S. & Emory, S.R. (1997) Probing single molecules and single nanoparticles by surface-enhanced Raman scattering. *Science*, **275**, 1102–1105.

Nieman, L.T., Krampert, G.M. & Martinez, R.E. (2001) An apertureless near-field scanning optical microscope and its application to surface-enhanced Raman spectroscopy and multiphoton fluorescence imaging. *Rev. Sci. Instrum.* **72**, 1691–1699.

Novotny, L., Sánchez, E.J. & Xie, X.S. (1998) Near-field optical imaging using metal tips illuminated by higher-order Hermite–Gaussian beams. *Ultramicroscopy*, **71**, 21–29.

Rao, A.M., *et al.* (1997) Diameter-selective Raman scattering from vibrational modes in carbon nanotubes. *Science*, **275**, 187–191.

Sánchez, E.J., Novotny, L. & Xie, X.S. (1999) Near-field fluorescence microscopy based on two-photon excitation with metal tips. *Phys. Rev. Lett.* **82**, 4014–4017.

Sick, B., Hecht, B. & Novotny, L. (2000) Orientational imaging of single molecules by annular illumination. *Phys. Rev. Lett.* **85**, 4482–4485.

Souza Filho, A.G., *et al.* (2002) Anomalous two-peak G′-band Raman effect in one isolated single-wall carbon nanotube. *Phys. Rev. B*, **65**, 085417–085425.

Stöckle, S.M., *et al.* (2000) Nanoscale chemical analysis by tip-enhanced Raman spectroscopy. *Chem. Phys. Lett.* **318**, 131–136.

Wessel, J. (1985) Surface-enhanced optical microscopy. *J. Opt. Soc. Am. B*, **2**, 1538–1540.

Xu, H., Aizpurua, J., Käll, M. & Apell, P. (2000) Electromagnetic contributions to single-molecule sensitivity in surface-enhanced Raman scattering. *Phys. Rev. E*, **62**, 4318–4324.

Yu, Z. & Brus, L.E. (2001) Rayleigh and Raman scattering from individual carbon nanotube bundles. *J. Chem. Phys. B*, **105**, 1123–1134.